Journal of Cultural Heritage 52 (2021) 55–64

Contents lists available at ScienceDirect

Journal of Cultural Heritage

journal homepage: www.elsevier.com/locate/culher

Original article

A comparative appraisal of Raman band ratioing and chemometric analysis for classification of ancient papyri

F.J. Pereira[a], R. López[a], N. Ferrer[b], A. Carmelo Prieto[c], R. Alvarez Nogal[d], A. Nodar[e], A.J. Aller[a,*]

[a] Department of Applied Chemistry and Physics, Faculty of Biological and Environmental Sciences, Campus de Vegazana, s/n, University of León, León, Spain
[b] Centres Científics i Tecnològics (CCiTUB), University of Barcelona, Barcelona, Spain
[c] Department of Condensed Matter Physics, Crystallography and Mineralogy, Faculty of Sciences, University of Valladolid, Spain
[d] Department of Molecular Biology, Faculty of Biological and Environmental Sciences, Campus de Vegazana, s/n, University of León, León, Spain
[e] Department of Humanities, University Pompeu Fabra, Barcelona, Spain

ARTICLE INFO

Article history:
Received 11 May 2021
Revised 4 August 2021
Accepted 7 September 2021
Available online 30 September 2021

Keywords:
Carbon-based inks
Vibrational spectroscopy
Multivariate analysis
SEM/EDX
FT-IR
Raman spectrometry

ABSTRACT

Papyri from past civilizations represent key information sources to understand historical societies and their culture. In general, the most critical information usually derives from the inks rather than the supports. In this work, we combine several analytical tools, including vibrational spectroscopies (FT-IR and Raman) and SEM/EDX spectroscopy, to characterise the inks of various papyri in the Palau-Ribes collection (Barcelona, Spain). The Raman spectra corroborate the presence of soot-based inks as the primary type. We use a five-peak spectral model for the deconvolution of the first-order region of the Raman spectra, which allows us to derive information about the carbon type of the soot-based inks. Further, we propose various Raman band ratios for a thorough evaluation of the graphitization process of carbon and possible classification of the ancient inks. At the same time, we use multivariate analysis, mainly assisted by cluster analysis, principal component analysis, and the Fisher discriminant functions, to enable an excellent alternative way to verify the classification and differentiation of the inks safely as a function of the historical time.

© 2021 The Author(s). Published by Elsevier Masson SAS.
This is an open access article under the CC BY-NC-ND license
(http://creativecommons.org/licenses/by-nc-nd/4.0/)

1. Introduction

Papyri have been widely used in the Mediterranean basin as a generalized means of knowledge transmission for about four millennia, especially during the Hellenistic and Roman periods (S. III BCE – VII CE). The Physico-chemical characteristics and stability of the inks and the papyrus supports, which largely depend on the historical period, contain valuable information about the ancient societies. The papyrus supports have a complex matrix, joining compounds with similar chemical structures, where cellulose, lignin and hemicellulose are the main constituents. Furthermore, the support material can degrade via oxidation, but the primary degradation mechanism is acid hydrolysis [1-3], breaking the chemical bonds usually through nucleophilic substitution. Nonetheless, the structural defects and environmental conditions, such as humidity, exposure to light, especially the iron content of the ink and the contact surface between support and ink, can alter the degradation process [4-6].

The inks traditionally used to write on papyri usually group within three categories: carbon, mixed and iron gall-inks [7]. The three types of ink contain carbon as an essential component, although it is mainly in the carbon-based inks and always mixed with different metalloids, metals and natural pigments [8]. Thus, the iron gall-inks incorporate soluble complexes formed between tannins and iron(II) [9], which by oxidation transform into water-insoluble iron(III) complexes [9,10]. Further, to improve the stability and colour of the inks, the addition of natural products has been common practice but its use changes with the historical period, geographical area and purpose of writing [11]. The previous statements highlight the significant analytical challenge for a complete characterisation of the ancient inks, mainly due to their complex matrix, linked to the need not to damage the papyri. Nonetheless, the variability in the ink composition can provide more diverse and detailed information about each historical period.

* Corresponding author at: Department of Applied Chemistry and Physics, Faculty of Biological and Environmental Sciences, Campus de Vegazana, s/n, University of León, E-24071 León, Spain
E-mail address: aj.aller@unileon.es (A.J. Aller).
URL: https://orcid.org/0000-0002-6454-7828 (A.J. Aller)

https://doi.org/10.1016/j.culher.2021.09.003
1296-2074/© 2021 The Author(s). Published by Elsevier Masson SAS. This is an open access article under the CC BY-NC-ND license
(http://creativecommons.org/licenses/by-nc-nd/4.0/)

Any systematic study of the inks using non-invasive physicochemical techniques might potentially shed light on their composition and consequently on their potential origin and the possible presence of degradation [1,12]. The main techniques used for this purpose include particularly those based on vibrational spectroscopy, such as Fourier Transform-InfraRed (FT-IR) spectroscopy [13,14] and particularly Raman spectroscopy [10-12,15,16]. Raman spectroscopy, however, is very sensitive to both crystallinity and molecular structures (short-range order), being usually the analytical tool of choice to study the structural disorder of the crystalline material. In this way, Raman spectroscopy is adequate to study historical objects, pigments and carbonaceous materials [16-18]. Additionally, scanning electron microscopy/energy-dispersive X-ray (SEM/EDX) spectroscopy and X-ray fluorescence, the last technique using many times synchrotron radiation for excitation [14,19,20], have also been used to obtain information about the elemental content [21-22].

According to their components, any possible classification or differentiation of the ancient inks is of great concern to establish potential historical correlations. In this respect, there are different statistical models capable of analysing vibrational spectra and elemental composition [13,21,23]. Thus, the linear discriminant analysis combined with SEM/EDX allowed us to differentiate between Roman and Byzantine inks [21]. Using near IR spectroscopy and partial least squares calibration facilitated the pH determination and the degree of polymerisation of the papyrus supports and inks [24]. However, to achieve this purpose, various spectral preprocessing procedures, such as standard normal variate, Savitzky–Golay digital filter and second derivative, have been widely incorporated to optimize the quality of the chemometrics models [25].

2. Research aim

This work aims to achieve a consistent chemical characterization of the inks of seven dated papyri in the Palau-Ribes collection (Barcelona, Spain), covering a broad historical period (I CE – VIII CE) using FT-IR and Raman spectroscopy, in combination with SEM/EDX.

This work also aims to find a possible means for dating and differentiating the ancient inks using Raman band ratios. For this purpose, we involve band areas, band intensities, and full-widths-at-half-maximum (FWHMs) of the five deconvoluted bands of the first-order region of the Raman spectra.

Finally, we compare the results obtained using the above age rating approach with those found through different multivariate analyses.

3. Material and methods

3.1. Material

The inks studied in the Palau-Ribes collection (Barcelona, Spain) (Fig. SI-1) come from the Byzantine period: VIII century (P. Palau Rib. Inv. 451), VII century (P. Palau Rib. inv. nos. 6, 14, 209), and the Roman period: II century (P. Palau Rib. inv. nos. 125), and I century (P. Palau Rib. inv. nos. 66, 158). The samples were dry cleaning by blowing pressurized air as the only treatment before analysis to avoid dust contamination.

3.2. Raman spectroscopy

A high-resolution LABRAN HR 800 UV micro-Raman spectrometer (Horiba-Jobin & Yvon Spex, France), equipped with an Olympus BX41 microscope (x100) and an XYZ motorized platen for automatic positioning and focalization of the sample, was used for dynamical-vibrational studies of ink particles of ng-size. This spectrometer includes a confocal system with 1200 lines/mm diffraction grating covering the spectral range 150-2200 cm^{-1}. The spectrometer incorporates a liquid N_2-refrigerated CCD Symphony detector, showing a maximum sensibility in the range of 500-850 nm. The excitation wavelength was the solid-state NdYAG unfolded laser at 532.1 nm. We adjusted the laser power in the range of 1-100% and the nominal power of the laser attenuated using a filter D0.3 up to 270±0.5 μW, with a maximum irradiance of 5 $kWcm^{-2}$. Under these experimental conditions, we assure the minimum invasive character of this technique. The acquisition time was in the range 0.5-60 s, an accumulation integration of 2 and bandwidths of 300 μm, resulting in a spectral resolution of 1 cm^{-1}. We calibrated the instrument using the Raman Stokes stretching vibration (Si-Si) at 520.7 cm^{-1} from a crystalline Si flat wafer ordered according to the crystallographic face (001).

We fitted the five component bands for calculating the Raman spectral parameters using the software LabSpec, © Horiba-Jobin&Yvon and Origin 9.0. The protocol of action started from the original Raman spectrum, under which the baseline generated reproduces the profile of the fluorescence band. A 3-9 degree polynomial baseline was adequate as a standard protocol, which generally coincides with a fluorescence band providing direct information about the material studied. We obtained the fluorescence-free Raman spectrum by comparing the experimental Raman spectrum and the estimated baseline. The mean square deviation indicated the goodness of fit, χ^2, showing potential values equal to unity in the case of an exact agreement, values in the range 1-3 some convergence and above 3 zero convergence.

3.3. FT-IR

We used an FT-IR Spectrometer THERMO IN 10 (Thermo Fisher Scientific, Waltham, MA, USA), equipped with a microscope and MCT detector, KBr beam splitter, and Glow Bar source. We placed the papyri and ink samples for analysis on a Specac's high-pressure Diamond Compression Cell, designed for in-compartment FT-IR spectroscopic transmission analysis. Up to 64 scans were co-added, using a 50 to 100 μm bandwidth and 4 cm^{-1} resolution. The spectra were baseline-corrected and normalized using the maximum-minimum normalization in the Origin 9.0 software to minimize problems from baseline shifts.

3.4. SEM/EDX

We performed electron microprobe analysis of the papyrus supports and inks in a JEOL Scanning Electron Microscope (Model JSM-6480LV), equipped with an energy-dispersive X-ray detection system (Oxford D6679 EDS detector), operated under recommended conditions (15 kV acceleration voltage and 5 nA probe current). After treating the sample with the electron beam for 100 s, we obtained each spectrum, whilst the working distance was 10 mm. Electron microprobe operated at 85 Pa to assure the physical integrity of papyri. We analyse the papyri directly.

3.5. Multivariate analysis

We used two statistical assays, the F-test, which requires a normal data distribution, and the non-parametric Kruskal-Wallis test, to check if each data set comes from different origins (inks). A 95% confidence level two-way ANOVA test allows us to evaluate the influence of two discrete independent variables (ink and wavenumber) on the dependent variable (absorbance). However, hypothesis testing in ANOVA assays by the F-test assumes a normal distribution of the data and equal residual variance in all treatment groups, which, if violated, losses of power can result. Nonetheless,

moderate deviations from normality are possible based on the central limit theorem, especially with few samples. In any case, to check a distribution close to normal, we also carried out the non-parametric Kruskal-Wallis test for comparison purposes.

We selected principal components analysis (PCA) as a well-established technique for reducing the dimensionality of the multivariate data. We linearly combined the original variables into orthogonal (independent) principal components (PCs). Only the most significant PCs were used but preserving most of the variance. The remaining PCs are presumed random *noise* in the data and ignored without reducing helpful information representing the data.

We also used Discriminant Function Analysis (DFA) to differentiate between groups based on the retained PCs. According to the Euclidean distance between groups in DFA space and following the primarily known hierarchical cluster analysis (HCA), an agglomerative clustering algorithm constructs a dendrogram. Dendrograms graphically represent the spectral similarities and classification of the objects (analytes) under study. We used the Origin 9.0 software to implement these methods. We select the wavenumber regions assayed, stated throughout the text, from the IR (normalized absorbance intensity) and Raman spectra according to the most representative functional groups.

4. Results and discussion

We included a previous characterisation of the papyrus supports by FT-IR spectroscopy (Fig. SI-2) in Supplementary Information for reference purposes. Furthermore, we also incorporated several crystallinity indexes to evaluate the crystallinity degree of the lignocellulosic material (Fig. SI-3).

4.1. Spectroscopic characterization of the inks

The FT-IR spectra of the inks (Fig. 1A, B) show a carbonyl IR region stronger than in the supports case (Fig. SI-2), which suggest a higher oxidation degree. Minor contributions from the papyrus supports are possible since the analyses of the inks were made directly without isolation from the support. Nonetheless, the IR spectra of both supports and inks differ, as stated in their derivative form in Fig. SI-2 (C). The ester function, related to the peak around 1710 cm^{-1}, was noted for all inks, whilst the carbonyl IR peak at ~1667 cm^{-1}, ascribed to α-diketones and α,β-unsaturated carbonyl groups, was mainly present in ink 6. Nonetheless, this peak, together with those at 1324, 797 and 775 cm^{-1}, also correlate with the presence of oxalates [26]. Furthermore, the OH stretching vibration picking around ~3400 cm^{-1} (Fig. 1A) is broader than the corresponding IR peak from the supports (Fig. SI-2A). The crystallization water provides narrow IR bands around 3633 and 3698 cm^{-1} due to the terminal OH groups weakly hydrogen-bonded to oxygens and an abroad maximum at 3350-3430 cm^{-1} related to the OH groups involved in water-to-water hydrogen bonding (Fig. 1A, Fig. SI-4). The overlapped weak peak around 1578 cm^{-1}, especially noted for the ink 451, is likely from alkenes, usually present in binders. Alkyl chains correlate with IR peaks at 1377-1411 cm^{-1} due to CH_2 bending and those attributable to CH sp^3 stretching at 2915 and 2847 cm^{-1}. Remarkably, the co-existence of the IR peaks at 2915, 1411 and 1377 cm^{-1} could suggest the typical binder gum Arabic [27], containing mainly D-galactose, L-arabinose, L-rhamnose and several organic acids, such as D-glucuronic and 4-O-methyl-D-glucuronic, although any other polysaccharide would also contribute. Gum Arabic acts as a suspension agent, facilitating the flow of the ink and inhibiting cellulose degradation. On the other hand, the IR region 1100-1500 cm^{-1} shows typical features of the aromatic rings.

Some IR peaks in the fingerprint region also relate to compounds involving some particular metals and metalloids. Thus, silicon, usually as SiO_2, typically generates IR peaks at 1070 and 797 cm^{-1} (Fig. 1B), together with the band at 1039 cm^{-1} assigned to the out-of-plane symmetric Si–O–Si mode. Nonetheless, the peak at 797 cm^{-1} also links to the C-SH bending vibrations [28]. A single Mg–O stretching band around 3698 cm^{-1} (Fig. 1A) ascribes to centrosymmetric hydroxyl groups [29]. Characteristic IR peaks at 1102 and 991 cm^{-1} (Fig. 1) originate from stretching vibrations of SO_4^{2-} ions [30,31], visible for the ink 6. On the other hand, the shoulder about 810 cm^{-1} (Fig. 1B) might attribute to acid sulphate ($-HSO_4-$) [32].

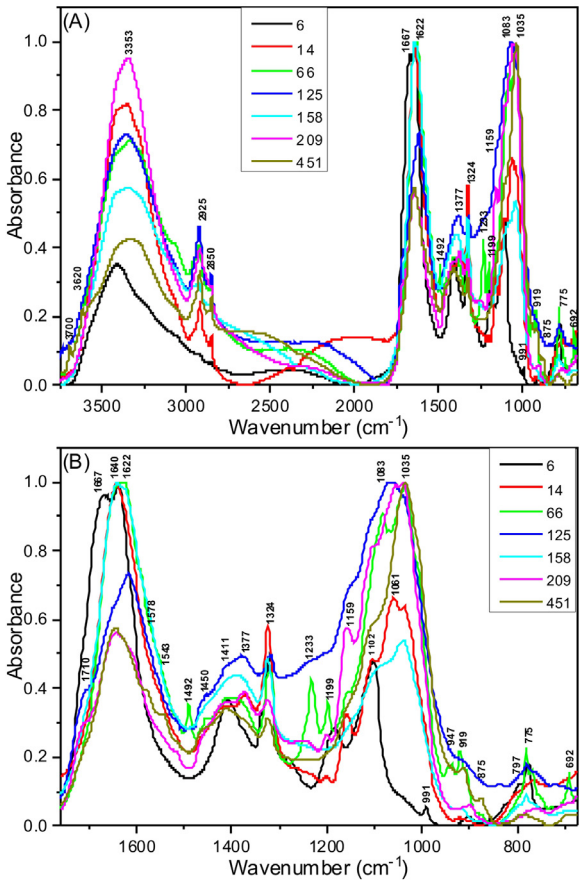

Fig. 1. (A) Normalized transmission FT-IR spectra of the seven inks studied. (B) Truncated FT-IR spectra from (A).

Notwithstanding, detection of the mentioned elements was better by SEM/EDX spectroscopy (Fig. 2, Fig. SI-5). Fig. 2 shows boxplots with the main elements found in the inks (and the corresponding supports for comparison) 6 (VII CE), 158 (I CE) and 209 (VII CE). It is worth noting the absence of lead and copper in the inks here studied; the absence of the last one facilitates a possible delay in the ageing process of the pigments [33]. The high potassium and calcium contents probably come from the raw materials, while phosphorous and sulphur link to the possible involvement of both organic and inorganic compounds. The aluminium, potassium, and silicon contents are higher in the inks than in the supports, showing some differences depending on the selected papyrus.

The iron content also predominates in ink against the support since some are exempt from this metal (Fig. 2). As a whole, the iron content in all inks studied is very similar (Fig. 3), although the most recent inks (Byzantine) have, on average, slightly higher iron levels than the inks from the first centuries (Roman). We used an internal reference to compensate for some possible changes to establish a tentative tool for rapid differentiation between Roman and Byzantine inks. Thus, taken the Ca content as an internal refer-

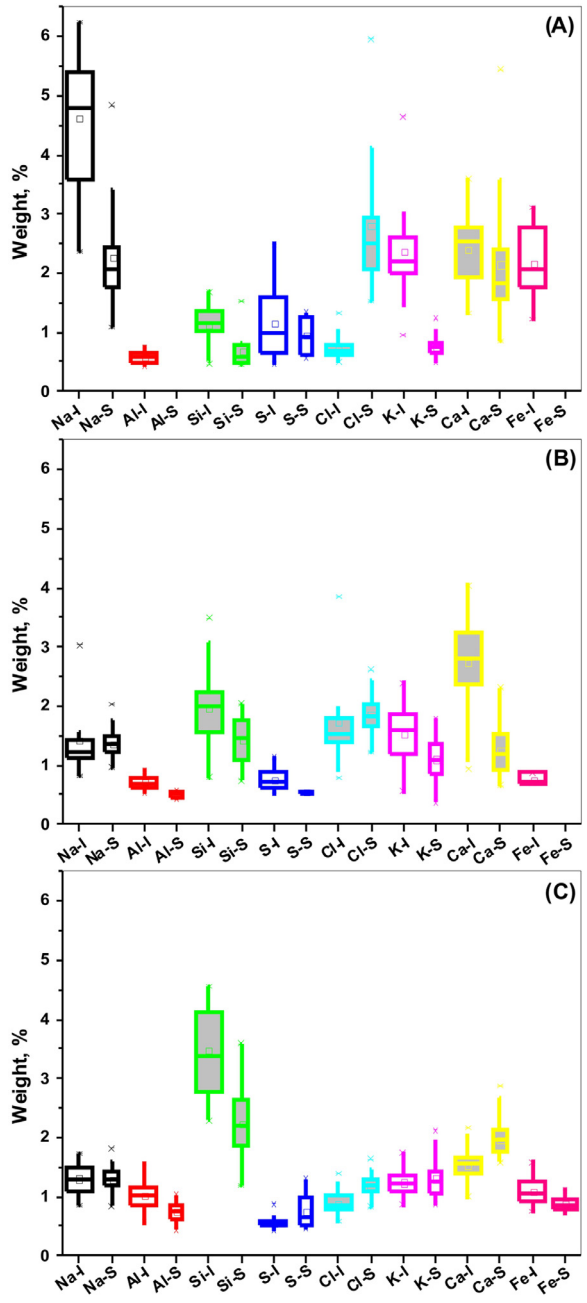

Fig. 2. Box-plots of the main elements found in the inks (I) and supports (S) for three representative papyri: (A) 6 (VII CE), (B) 209 (VII CE) and (C) 158 (I CE).

ence, we found that the highest proportions of some elements (Na, Fe) predominate in the Byzantine period, while others (Si, Al) are similar (Fig. 3). Contrarily, the content of calcium is always higher in the Roman inks. We choose calcium as a reference because it shows a precise opposite or positive correlation with the other selected elements for the Roman and Byzantine periods (Table SI-1, Table SI-2). Only iron show a similar positive correlation for both periods (Table SI-1 and Table SI-2). These plots or any other similar are valuable tools to establish initial pictorial differences between the Roman and Byzantine inks.

Micro-Raman spectroscopy provided additional light to the ink composition using the ink-free papyrus as a pictorial substrate and instrumental blank. Fig. 4A shows the micro-Raman spectra of the black inks 6 (VII CE) and 209 (VII CE), which are comparable to those obtained by other authors [34] for other papyri. All Raman spectra (Fig. SI-6) show intense bands in the first-order Raman region 1100–1800 cm^{-1}, which characterise the carbon-based inks [10,12,15,34-38]. The two strong, broad peaks of the first-order Raman region picking at 1360 and 1570 cm^{-1} (Fig. 4A, B) ascribe to the C-C stretching vibrations within the polyaromatic structure of little organized carbonaceous material. Conclusively, the carbon black inks of this work mainly contain the smoke black pigment (soot or amorphous carbon), although with minor amounts of some metals and metalloids. In other words, the main constituent is carbon structurally disordered by network imperfections, mixed with minor contents of some organic and inorganic compounds [34,39], suggesting a plant origin. The inks studied cannot be grouped as typical iron-gall inks, firstly because the Raman spectra do not show the typical features of the iron-gall inks, and secondly, the iron levels, similar to those of calcium and potassium, are only a little higher than those found for the corresponding supports. However, the typical iron-gall inks have iron contents at least ten times higher than the supports [15,22,40-43].

According to the following degradation sequence, the original carbonaceous material of the black inks degrades nanocrystalline graphite, amorphous carbon and sp^3 tetrahedral amorphous carbon, whose typical features display in the Raman spectra. The best way to know the degree of graphitization of the carbon black inks is by deconvolution of the two broad bands at 1360 and 1570 cm^{-1} (Fig. 4B) [44,45] and the use of various integrated areas ratios (Table SI-1). To better understand the inks' graphite type, we used a spectral model of five bands to deconvolution the Raman spectra' first-order region [38,46]. The five-band spectral deconvolution model incorporates four Gaussian-Lorentzian bands (G, D_1, D_2, D_4) ideally located around 1580, 1350, 1620, and 1200 cm^{-1}, respectively, and a fifth Gaussian band (D_3) at ~1500 cm^{-1} (Fig. 4B). These five-component bands are the most appropriate to evaluate the first-order Raman spectra of the carbon black ink, although their relative positions and intensities are sensitive to the excitation wavelength due to the resonance effect [47,48]. The G band, arisen from the doubly degenerate zone centre phonons of E_{2g} symmetry, appeared in this work at 1562-1581 cm^{-1} (theoretically in the range 1500-1630 cm^{-1}). This band results from the contribution of in-plane stretching vibration of any pair of C sp^2 atoms in both aromatic and olefinic molecules, although the sp^2 chains alone raise this band even up to 1690 cm^{-1} [35,49]. The D_1 defect band (K-point phonons of A_{1g} symmetry), providing Raman shifts at 1348-1367 cm^{-1}, comes from the breathing mode of sp^2 atoms (C=C bonds) in clusters of about six-fold aromatic rings [49]. The D_1 band only appears in the presence of in-plane defects, edges (as oxides), disorders [45], and metals and metalloids [50]. The Raman shift of the D_2 band, falling in the range 1601-1611 cm^{-1}, typically derives from high contents of oxidised sp^2 carbons, graphite intercalation compounds, and trace amounts of residual mono- or di-benzene species [51]. The D_3 defect band, covering values 1464-1531 cm^{-1}, relates to very poorly crystallized (amorphous) graphite. The intensity of the D_3 band decreases with oxidation of the amorphous carbon, which usually oxidizes more quickly than the graphitic crystallites. Finally, the D_4 band, which appeared in the range 1181-1279 cm^{-1}, assigns to sp^2-sp^3 bonds or C-C and C=C stretching vibrations of polyene-like structures (hydrocarbons or aliphatic moieties embedded on the disordered carbon network).

4.2. Assessing Raman band ratios for grouping of the inks

Different processes, such as the manufacturing process and thermal and oxidative stress, are responsible for graphite disorder, increasing with time. The age of the papyri encompasses the whole contribution of all factors affecting degradation. To evaluate the degree of the disorder, we can use several parameters from

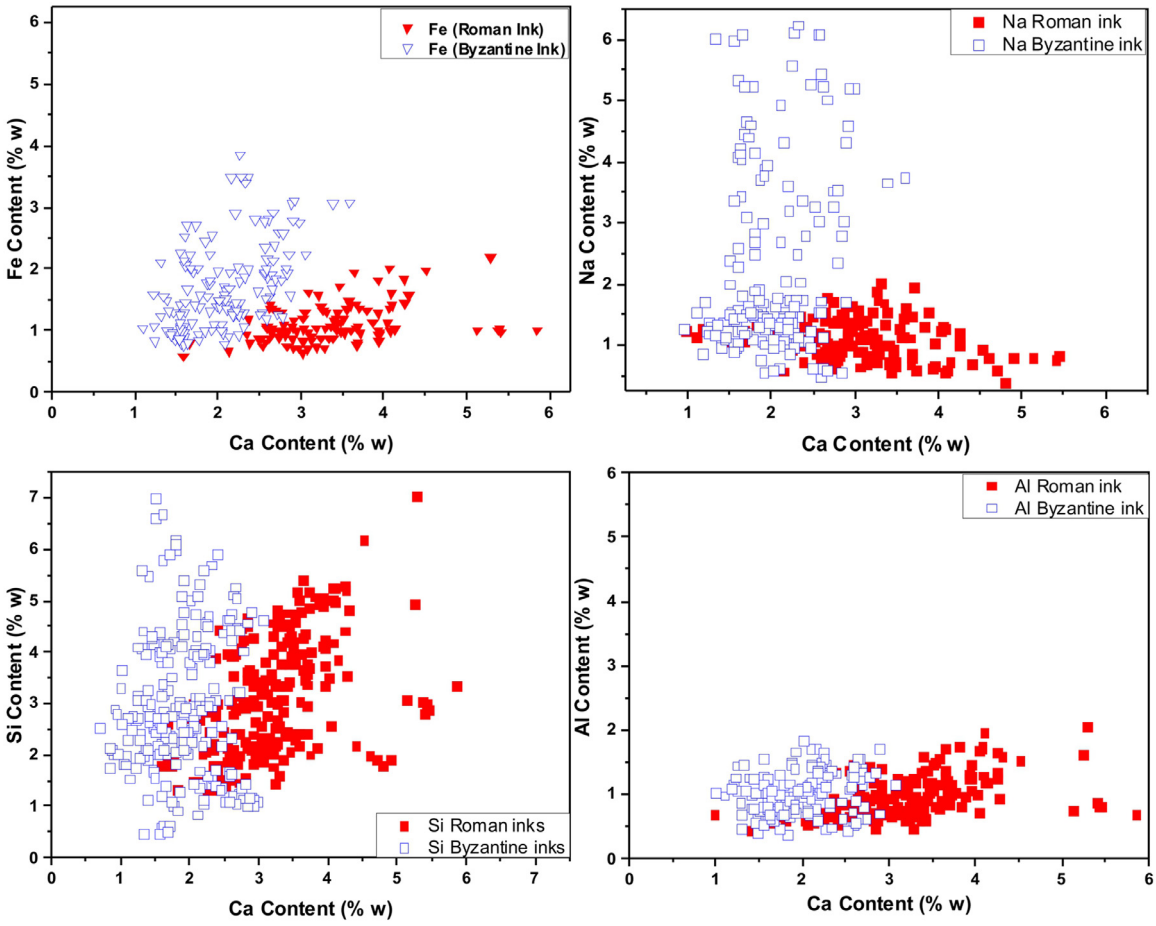

Fig. 3. Content of Fe, Na, Si, and Al versus the content of Ca for the Roman and Byzantine papyri.

the Raman spectra. Among them, the full-widths-at-half-maximum (FWHM) fundamentally of the *D* and *G* bands, the Raman shifts of the deconvolution bands, intensity/FWHM ratios and any other possible relationship can provide information about the state of degradation. From the deconvolution bands, only D_4 shows some shift with age (Fig. SI-7), while the positions of the *G* and the other *D* bands are nearly constant (Fig. SI-7). The range of the Raman shifts of the D_1 (1367-1348 cm^{-1}) and *G* (1581-1562 cm^{-1}) bands range equally, denoting some graphitization and suggesting the presence of an amorphous phase with a high sp^2/sp^3 ratio.

On the other hand, Fig. SI-8 displays the FWHM values of the *G* and D_i bands versus the corresponding Raman shifts. Fig. SI-8 shows that the D_1 and *G* widths cover a narrower range of wavelengths than the other peak (D_2, D_3, D_4). Further, the widths of the Roman papyri (66, 125, 158) take values closer to each other than the Byzantine ones (6, 14, 209, 451). In addition, the D_4 bands show a blue shift for some of the Byzantine papyri (Fig. SI-7, Fig. SI-8). Some authors have established relationships between the *G*-band position and its FWHM [52]. Thus, large values of $FWHM_G$ and a *G* band position above 1580 cm^{-1} indicate significant structural disorder in the presence of the D peaks [53]. However, in this work, we have never found *G* band positions beyond 1580 cm^{-1} (Fig. SI-8). As the defects increase, nanocrystalline graphite forms and the *G* band is blue-shifted [10,24,25], although to a small extent in this work (Fig. SI-8). The average dispersion values of $FWHM_{Di}$ vary according to $D_3 > D_2$, $D_4 > D_1$ (Fig. SI-8), which suggests the predominance of the amorphous carbon, oxidised sp^2 and sp^2-sp^3 bonds (polyene-like structures), as highlighted above for each deconvolution Raman band.

For a more detailed assessment of the degradation degree of the carbonaceous material of the inks and their possible classification, we first evaluated several integrated area ratios (RA_1, RA_2, R'_2 and R'_3) (Table SI-3), widely used in other fields [54], which involve a mixed contribution from various of the five deconvolution bands. Thus, di-benzene species (from D_2) together with amorphous (from D_3) and defect-free (from *G*) carbon contribute in more significant extension than the very disordered network and metals according to the small values of RA_1 (Table SI-3). The values found for RA_1 larger than 0.5 indicate that the contribution from D_1+D_4 would be more significant than that of D_2+D_3+*G*. Similar information would provide the values of RA_2 above the unity, indicating significant contributions from D_1 and D_4 compared to D_2+D_3+*G*. Alternatively, if the contribution of D_1 matches that of *G*+D_2, the parameter R'_2 would take values around 0.5. Similarly, for R'_3 but considering the contribution from D_3 instead of D_2. According to these results (Table SI-3), amorphization of the carbonaceous material would be the leading cause of degradation of the inks 6 (VII CE), 66 (I CE), 125 (I CE), 14 (VII CE) and 451 (VIII CE), whilst the inks 158 (I CE) and 209 (VII CE) would suffer more substantial degradation from the presence of metal(loid)s. Nonetheless, most of the integrated area ratios (RA_1, RA_2, R'_2 and R'_3) included in Table SI-3 vary within a very narrow range, making it challenging to interpret small changes between papyri.

Consequently, alternative band ratios are worth using based on the deconvolution bands' intensity (peak height) to solve this problem and for a more thorough evaluation of the degradation process. Thus, the following intensity ratios, $R_1=I_{D1}/I_G$, $R_2=I_{D2}/I_G$, $R_3=I_{D3}/I_G$, and $R_4=I_{D4}/I_G$ (abbreviated $R_i = I_{Di}/I_G$, where $i = 1, 2, 3, 4$) remark the contribution of each deconvolution Raman peak,

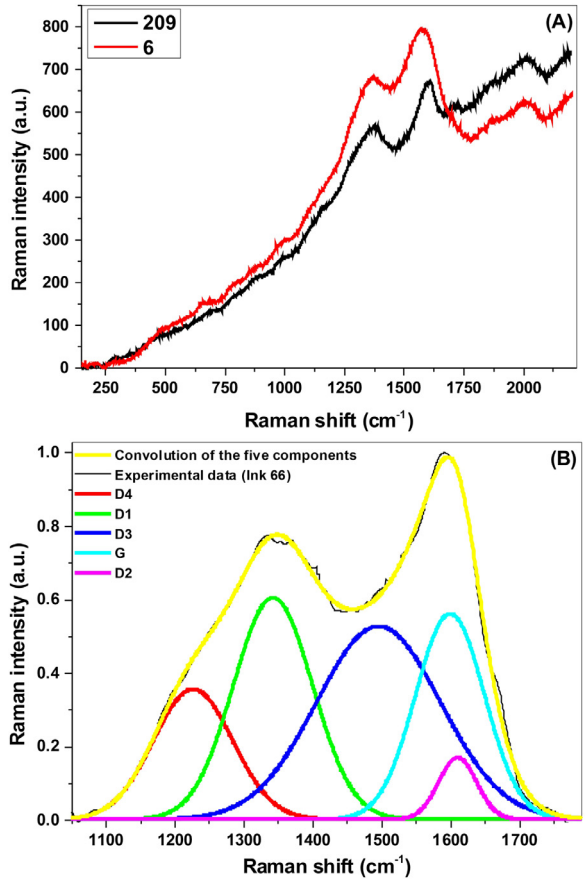

Fig. 4. (A) Original micro-Raman spectra of the inks 6 (VII CE) and 209 (VII CE). (B) A truncated micro-Raman spectrum of the ink 66 (I CE) and its spectral decomposition in the five deconvolution Raman bands (*G*, D_1, D_2, D_3 and D_4) with their convolution band.

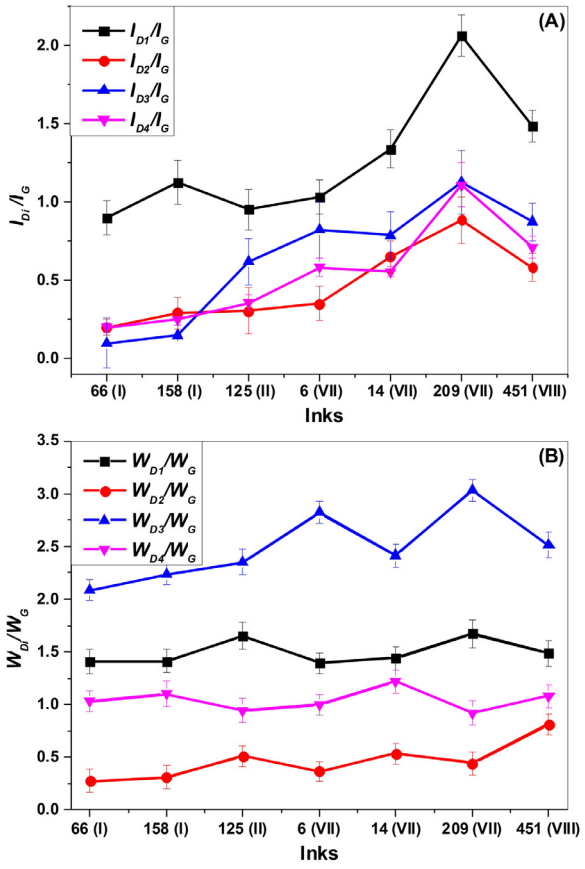

Fig. 5. Intensity ratios (A) and FWHM ratios (B) versus the seven papyri studied.

taken as reference the non-degraded material (*G* peak). These intensity ratios show an apparent inverse relationship with the papyri age (Fig. 5A) and can be used to characterize intermediate- and high-grade graphite [55]. Each R_i ratio from the same papyri can show some differences from one sampling spot to another due to the usual measurement errors and minor heterogeneities usually present in these samples, but they do generally not confirm the existence of different types of inks [56]. The R_1 ratio, which thrives with the formation of sp^3-bonded carbon-hydrogen clusters, graphite edges, and small aromatic ring clusters [45], ranges between 0.9 and 2.0, indicating structural disorder and measuring the defect density of the graphite. Values of R_1 above unity suggests some participation of metals in the graphitization process. Contrarily, small values of R_2, R_3 and R_4 means relatively minor amounts of oxidised sp^2 carbons, amorphous graphite, and low levels of polyene-like structures, respectively. According to the values of the different R_i ratios of this work, the ink 209 (VII CE) suffered an intense disorder of the graphite network compared with ink 6 (VII CE), which contains more significant amounts of defect-free crystalline graphite. On the other hand, the amount of residual carbonaceous species (mono- and di-benzene species) in ink 14 (VII CE) is higher than in ink 6 (VII CE). As a whole, the I_{Di}/I_G ratios take smaller values for the Roman inks than for the Byzantine inks (Fig. 5A). Thus, the I_{D1}/I_G ratios take values around and above unity 1.0 for Roman and Byzantine inks, respectively, whilst the other intensity ratios (R_2, R_3 and R_4) have values always below (Roman) and above (Byzantine) 0.5.

Alternative to the intensity ratios, we also assayed the FWHM relationships to characterise the carbonaceous material. However, the $FWHM_G$ and $FWHM_{Di}$ values grow with the structural disorder, excitation wavelength and type of carbon [35,49,57]. For this reason, the use the $FWHM_{Di}/FWHM_G$ ratios (Fig. 5B) is better to provide more accurate values because both $FWHM_{Di}$ and $FWHM_G$ would experience the same possible alteration compensating each other. Fig. 5B shows the $FWHM_{Di}/FWHM_G$ (or W_{Di}/W_G) ratios against the inks, providing W_{D2}/W_G and W_{D3}/W_G growth particularly the last one, similarly to the information found in Fig. 5A.

Notwithstanding, we also used other plots to establish reliable groupings tentatively. Thus, the I_{Di}/I_G and W_{Di}/W_G ratios versus W_{Di} (Fig. 6) show that the Roman inks (66, 125, 158) are more closely grouped compared to the Byzantine ones (6, 14, 209, 451). The best differentiation between both types of inks (Roman and Byzantine) results using the I_{D4}/I_G (Fig. 6A) and W_{D1}/W_G (Fig. 6B) ratios, although the other two I_{D1}/I_G (Fig. 6A) and W_{D4}/W_G (Fig. 6B) ratios also provide helpful information. Thus, the older inks showed smaller values of W_{D4} for the I_{D4}/I_G (Fig. 6A) and W_{D4}/W_G (Fig. 6B) ratios and higher values of W_{D1} for the I_{D1}/I_G (Fig. 6A) and W_{D1}/W_G (Fig. 6B) ratios. In summary, this type of plot may be suitable for establishing a clear differentiation between the Roman and Byzantine inks.

4.3. Chemometric analysis

To establish differences in the origin of the inks, we compared the IR spectra of the inks in the wavenumber range 700-1800 cm^{-1} using a two-way analysis of variance. The *p*-values (0.01) derived from this analysis (Table 1) indicate dissimilarity between the IR spectra of the inks. Differences in the IR spectra appear not only in the maximum absorbance but also in the neighbouring wavenumbers. A few inks show qualitative similarity in their chemical composition but quantitative differences, allow-

Table 1
Correlation matrix showing *p*-values of the two-way ANOVA test (top box) and the Pearson correlation coefficient (bottom box) for the seven inks evaluated.

Inks	66 (I)	158 (I)	125 (II)	6 (VII)	14 (VII)	209 (VII)	451 (VIII)
66(I)		0.49836	0.08800	0.35200	0.21269	0.18500	0.22570
		0,89794	0,94216	0,58354	0,92931	0,93029	0,96496
158(I)			0.30298	0.40774	0.21079	0.23490	0.38900
			0,90111	0,80641	0,83483	0,88518	0,93952
125(II)				0.73025	0.24300	0.03200	0.08200
				0,60599	0,91860	0,99053	0,98118
6(VII)					0.61205	0.41230	0.66583
					0,47934	0,58393	0,64526
14(VII)						0.13400	0.05100
						0,93592	0,94925
209(VII)							0.08700
							0,98177
451(VIII)							

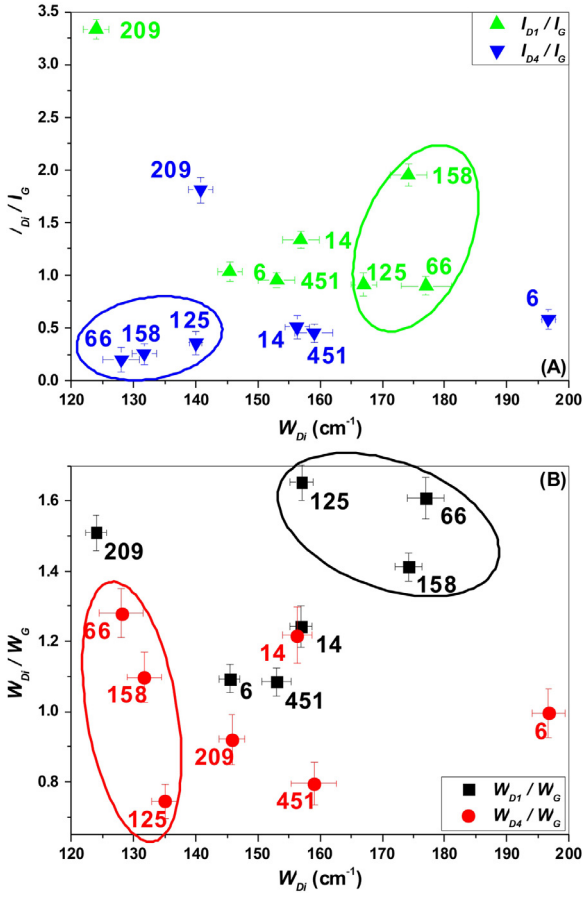

Fig. 6. The I_{Di}/I_G intensity ratios (A) and W_{Di}/W_G ratios (B) versus the W_{Di} of each defect peak where *W* is synonymous with FWHM.

ing the conclusion that the papyri studied derive from populations significantly different at the 0.05 significance level (Chi-Square: 290.18471; DF: 6; Prob>Chi-Square: 1.03618E-59). Notwithstanding, to avoid the normality distribution of the samples, we also applied the non-parametric Kruskal-Wallis test, reaching the same conclusion.

On the other hand, checking wavenumber regions between 700 and 1800 cm^{-1} from the FT-IR data and similarly using the second derivative Raman spectra, the Pearson correlation coefficients (Table 1) show relationships between inks similar to those derived from the two-way ANOVA test. The matrix correlation allows us to visualize associations existing among the inks by preserving the overall coherence of the dataset. No positive correlations ($p < 0.01$) turned out between the inks, indicating dissimilarity in their chemical composition. The Kaiser-Meyer-Olkin value was 0.789, while Barlett's test of sphericity (951.70) reached statistical significance ($p < 0.001$), which support the factorability of the correlation matrix.

The grouping process using PCA was coherent as a whole (Fig. 7). Using the same spectral regions from the Raman and FT-IR spectra, we can derive 3D plots with a clear grouping of the inks (I) and supports (S) (Fig. 7). Fig. 7A shows that the positive values of PC1 (46.3%) contribute enormously to the inks and the negative values to the supports. However, a less uniform response presents the contribution of PC2 (18.2%) and PC3 (13.3%). Fig. 7B shows that the FT-IR spectroscopy data provide a narrower grouping between supports than between inks. The contrary derives from the Raman data (Fig. 7A), which explains that the peaks of the Raman spectra come from constituents, mainly inorganic, differing in both supports and inks. However, the FT-IR spectra show intense peaks due to similar organic functional groups in both supports and inks. Grouping of the inks alone according to their historical time was also possible using Raman spectroscopy (Fig. 7C), with similar results to those found using the Raman band ratios (W_{Di}/W_G and I_{Di}/I_G ratios) (Fig. 6B).

Notwithstanding, the plots using two principal components (PC) with eigenvalues exceeding 1, explaining ~97% variance, show the inks and supports separately grouped (Fig. 8A, Fig. SI-9). The lines in Fig. 8A show the projections of the original data onto the PC axis. Positively correlated variables come together, while those negatively correlated are on opposite sides of the plot origin. In these plots, the distance to the origin measures the quality on the factor map. Thus, the further away from the origin, the better represented. A similar positive contribution of PC 1 (87.00% variance) to both the supports and the inks was evident, representing the fundamental contribution from the standard organic components present in the inks and supports. However, apparent differences appeared for the PC 2 (10.20% variance) contribution, positively for the inks and negatively for the supports, which would result from differences in the metal and metalloid contents in both inks and supports. However, individual differences between the inks also exist (Fig. 8A). The group of the supports is very close, which points to some similarity in their components. Contrarily, the group of the inks is more expanded, where the ink 6 (VII CE) differs concerning the ink 158 (I CE), and much more with the other inks, which agrees with the results set presented in the previous sections. Using the Raman range 1000-1800 cm^{-1}, a clear grouping of the Roman inks (66, 125, 158) was also possible (Fig. SI-10).

HCA allows us to classify the samples according to their similarities in chemical composition. Dendrograms from HCA render statistically significant clusters depending on the D_{link}/D_{max} ratio selected (Fig. 8B). Fig. 8B shows a dendrogram using the FT-IR spec-

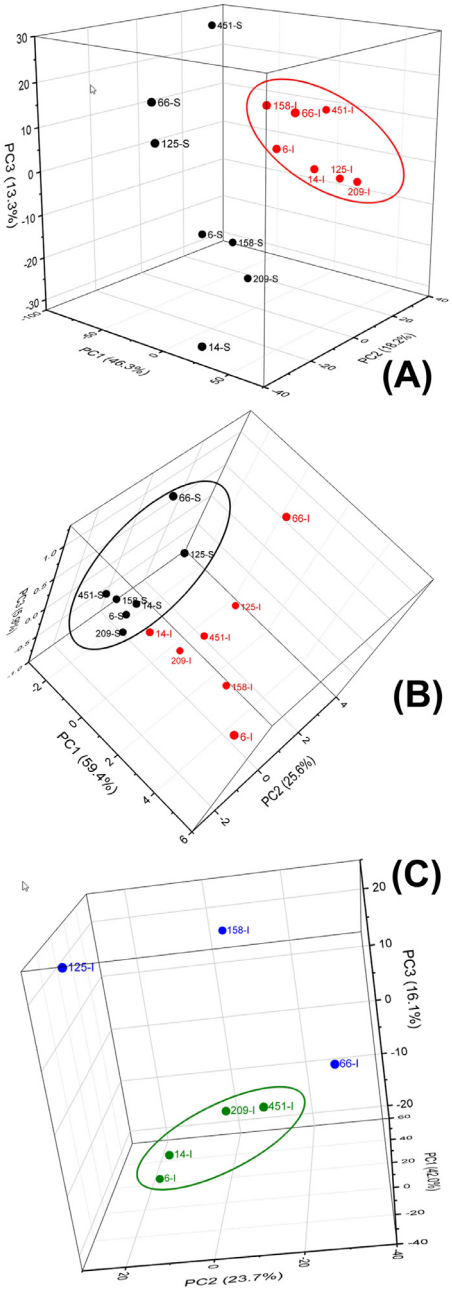

Fig. 7. 3D plots show a grouping of the inks (I) and supports (S) using 2nd derivative Raman spectra (700-1800 cm^{-1}) (A) and transmission FT-IR (700-1800 cm^{-1}) (B). (C) Grouping inks alone using 2nd derivative Raman spectra (700-1800 cm^{-1}) where the blue and green colours represent Roman and Byzantine inks, respectively. Inside and outside the circles are the inks or supports from the same period.

tra range 700-1800 cm^{-1}, illustrating a clear differentiation between the inks and the papyrus supports. Thus, a shorter distance linkage appeared for the inks 66 (I CE), 125 (II CE) and 158 (I CE), which constitutes the first group, including the older inks (Roman inks). Meanwhile, the distance linkage is much more than twice the others for inks 6 (VII CE) and 14 (VII CE), remarked by the significant difference in their chemical composition. There is also some similarity between the inks 209 (VII CE) and 451 (VIII CE), showing a short distance linkage. Nonetheless, the distance linkage between the papyrus supports is shorter, representing a logical situation as above stated. Alternatively, HCA allows us to group the inks according to age, using Raman and FT-IR spectroscopies (Fig. 9).

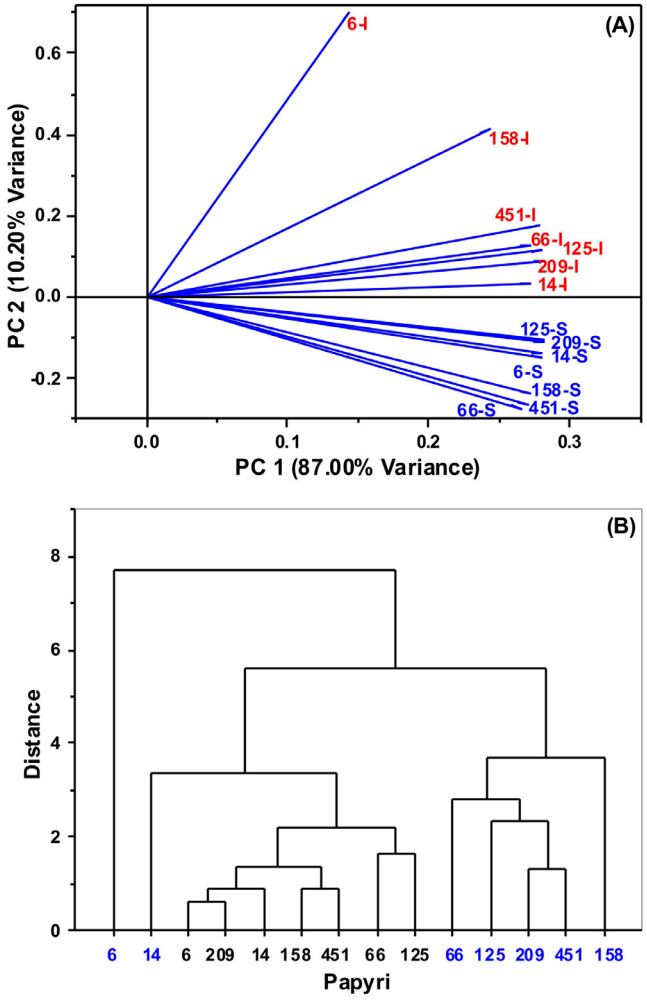

Fig. 8. (A) 2D plot using the FT-IR range 700-1800 cm^{-1} showing the grouping of the inks (I) and supports (S). (B) Dendrograms showing a Euclidean distance applied to the FT-IR spectra range 700-1800 cm^{-1} from the supports (in black) and inks (in blue)

Notwithstanding, to improve the chances of the best differentiation between Roman and Byzantine inks, we used the general linear discriminant analysis (LDA) to look for a linear combination of variables [21], finding prediction equations for differentiation between the inks. Applying the discriminant function of Fisher, we found several IR and Raman bands very adequate statistically for establishing significant differences between the Roman and Byzantine inks. Thus, we carried out LDA using intensity peak ratios and FWHMs of four IR bands selected at 1375-1400 cm^{-1} (Peak 1), 1635-1640 cm^{-1} (Peak 2), 2910-3000 cm^{-1} (Peak 3), and 3335-3410 cm^{-1} (Peak 4). We found two types of equations for the discrimination and classification of the inks. First, two classificatory approaches are possible using intensity ratios, or FWHM of the IR mentioned peaks, according to the equations,

$$F_{IR}^{I} = -7.514 + 3.473\ (I_{Peak\ 4}/I_{Peak\ 3}) \quad (1)$$

and

$$F_{IR}^{W} = -18.397 + 0.053\ (W_{Peak\ 4}) \quad (2)$$

The parameter F_{IR}^{I} takes values below zero for the Roman inks and above zero for the Byzantine inks. However, the contrary occurs using the parameter F_{IR}^{W}.

Alternatively, we also arrived at the two following equations using intensity ratios of the IR peaks 4 and 3,

$$Z_{IR}^{I} = -21.971 + 22.658\ (I_{Peak\ 4}/I_{Peak\ 3}) \quad (3)$$

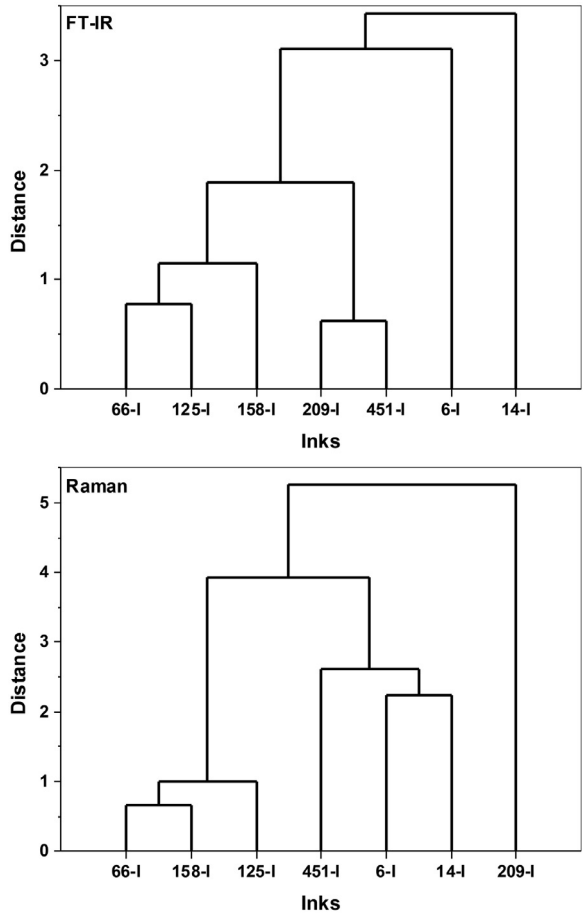

Fig. 9. Dendrograms grouping the Roman (66, 125, 158) and Byzantine (6, 14, 209, 451) inks using Euclidean distances applied to the FT-IR spectra range 1300-1700 $cm^{-1,}$ and the Raman spectra range 1000-1800 cm^{-1}.

$$\boldsymbol{Z_{IR}^{I\prime}} = -34.782 + 28.680\ (\boldsymbol{I_{Peak\ 4}/I_{Peak\ 3}}) \quad (4)$$

On this occasion, when we applied Eqs. (3) and (4) to one ink, if $\boldsymbol{Z_{IR}^{I} > Z_{IR}^{I\prime}}$, the ink is classified as Roman, while we grouped the ink as Byzantine if $Z_{IR}^{I} < Z_{IR}^{I\prime}$.

On the other hand, we can also use the FWHM of the IR peak 4, and according to the LDA, we found the two following equations,

$$\boldsymbol{Z_{IR}^{W}} = -187.760 + 1.034\ (\boldsymbol{W_{Peak\ 4}}) \quad (5)$$

$$\boldsymbol{Z_{IR}^{W\prime}} = -157.130 + 0.945\ (\boldsymbol{W_{Peak\ 4}}) \quad (6)$$

Similarly, as above, we applied Eqs. (5) and (6) to one ink. If $\boldsymbol{Z_{IR}^{W} > Z_{IR}^{W\prime}}$, the ink is considered as Roman, while it would be Byzantine if $Z_{IR}^{W} < Z_{IR}^{W\prime}$.

We also used the Fisher discriminant functions to group the inks but working with intensity peak ratios of two Raman bands selected at 1330 cm^{-1} (Peak 1) and 1590 cm^{-1} (Peak 2). We found the following equation,

$$\boldsymbol{F_R^I} = -31.072 + 25.031\ (\boldsymbol{I_{Peak\ 2}/I_{Peak\ 1}}) \quad (7)$$

The parameter $\boldsymbol{F_R^I}$ of Eq. (7) takes values above zero for the Roman inks and below zero for the Byzantine inks. Nonetheless, the two following equations are also possible,

$$\boldsymbol{Z_R^I} = -518.568 + 805.577\ (\boldsymbol{I_{Peak\ 2}/I_{Peak\ 1}}) \quad (8)$$

$$\boldsymbol{Z_R^{I\prime}} = -457.865 + 756.893\ (\boldsymbol{I_{Peak\ 2}/I_{Peak\ 1}}) \quad (9)$$

When we applied Eqs. (8) and (9) to one ink, if $\boldsymbol{Z_R^I > Z_R^{I\prime}}$, the ink is Roman, whilst it is Byzantine on the contrary situation, $Z_R^I < Z_R^{I\prime}$. Results from this work show LDA as a useful statistical tool for the successful classification of the inks.

5. Conclusions

Vibrational spectroscopies and SEM/EDX behaved properly as surface and subsurface analysis techniques to obtain critical information about the chemical composition of the inks. The first difference between inks was establishing plots with several elements against calcium as a reference, where aluminium, silicon, sodium and iron content make the difference. Nonetheless, with various intensity and width ratios of the deconvolution Raman bands, micro-Raman spectroscopy resulted in powerful approaches for characterizing and grouping the inks. Thus, the low-intensity ratios (R_i) relate to the Roman inks, whilst the high values of R_i concern Byzantine ones. Similarly, the smaller values of W_{D4} correlate with the smaller values of $I_{D4}/_{IG}$ and W_{D4}/W_G, whilst the higher values of W_{D1} with the higher values of I_{D1}/I_G and W_{D1}/W_G. Conclusively, the use of intensity ratios and width ratios could provide utility for the characterisation of ancient inks.

On the other hand, sorting by the age of the inks was also reasonably possible by PCA, HCA, and Fisher's discriminant functions, which proves that multivariate analyses help and complement other analytical tools. Conclusively, the most likely ink found in this work turned out to be like the soot-ink type, mixed with different small amounts of metals and metalloids (mixed inks). Notwithstanding, additional research is adequate to fine-tune the proposed methodology.

Author Contributions

AJA wrote the main manuscript text and managed the research data. AN checked the papyri characteristics. RAN carried out the SEM measurements. FJP performed the Raman and ATR-FTIR measurements. AC performed the micro-Raman measurements. NF carried out the transmission FT-IR measurements. AJA, RL and FJP evaluated the Roman band ratios and multivariate analysis. All authors discussed the results.

Acknowledgements

The financial support of Ministerio de Ciencia, Innovación y Universidades (Spain) by means of the grant with reference no. PGC2018-096572-B-C21 is gratefully acknowledged.

Supplementary materials

Supplementary material associated with this article can be found, in the online version, at doi:10.1016/j.culher.2021.09.003.

References

[1] J. Łojewska, I. Rabin, D. Pawcenis, J. Bagniuk, M.A. Aksamit-Koperska, M. Sitarz, et al., Recognizing ancient papyri by a combination of spectroscopic, diffractional and chromatographic analytical tools, Sci. Rep. 7 (2017) 1–12, doi:10.1038/srep46236.
[2] C. Corsaro, D. Mallamace, J. Łojewska, F. Mallamace, L. Pietronero, M. Missori, Molecular degradation of ancient documents revealed by 1 H HR-MAS NMR spectroscopy, Sci. Rep. 3 (2013) 1–10, doi:10.1038/srep02896.
[3] T. Łojewski, K. Zi¸ Eba •, A. Knapik, J. Bagniuk, A. Lubá Nska •, J. Łojewska, Evaluating paper degradation progress. Cross-linking between chromatographic, spectroscopic and chemical results, Appl Phys A 100 (2010) 809–821, doi:10.1007/s00339-010-5657-5.
[4] J.J. Lucejko, M.P. Colombini, E. Ribechini, Chemical alteration patterns of ancient Egyptian papyri studied by Pyrolysis-GC/MS with in situ silylation, J. Anal. Appl. Pyrolysis. 152 (2020) 104967, doi:10.1016/j.jaap.2020.104967.
[5] J. Malesic, J. Kolar, M. Strlič, in: Effect of pH and carbonyls on the degradation of alkaline paper: Factors affecting ageing of alkaline paper, Saur Verlag, 2002, pp. 145–153, doi:10.1515/REST.2002.145.

[6] B. Kanngießer, O. Hahn, M. Wilke, B. Nekat, W. Malzer, A. Erko, Investigation of oxidation and migration processes of inorganic compounds in ink-corroded manuscripts, Spectrochim. Acta - Part B At. Spectrosc. 59 (2004) 1511–1516, doi:10.1016/j.sab.2004.07.013.

[7] T. Christiansen, Manufacture of black ink in the ancient Mediterranean, Bull. Am. Soc. Papyrol. 54 (2017) 167–195 https://www.jstor.org/stable/44972209.

[8] K. Nesmerak, K. Nesměrák, I. Němcová, Dating of Historical Manuscripts Using Spectrometric Methods: A Mini-Review, Anal. Lett. 45 (2012) 330–344, doi:10.1080/00032719.2011.644741.

[9] C. Krekel, The chemistry of historical iron gall inks, Int J Forensic Docum Exam 5 (1999) 54–58.

[10] A.S. Lee, P.J. Mahon, D.C. Creagh, Raman analysis of iron gall inks on parchment, Vib. Spectrosc. 41 (2006) 170–175, doi:10.1016/j.vibspec.2005.11.006.

[11] D. Kurouski, S. Zaleski, F. Casadio, R.P. Van Duyne, N.C. Shah, Tip-enhanced raman spectroscopy (TERS) for in situ identification of indigo and iron gall ink on paper, J. Am. Chem. Soc. 136 (2014) 8677–8684, doi:10.1021/ja5027612.

[12] L. Burgio, R.J.H. Clark, Comparative pigment analysis of six modern Egyptian papyri and an authentic one of the 13th century BC by Raman microscopy and other techniques, J. Raman Spectrosc. 31 (2000) 395–401, doi:10.1002/1097-4555(200005)31:5⟨395::AID-JRS527⟩3.0.CO;2-E.

[13] T. Trafela, M. Strlič, J. Kolar, D.A. Lichtblau, M. Anders, D.P. Mencigar, et al., Nondestructive analysis and dating of historical paper based on IR spectroscopy and chemometric data evaluation, Anal. Chem. 79 (2007) 6319–6323, doi:10.1021/ac070392t.

[14] T. Arlt, H.E. Mahnke, T. Siopi, E. Menei, C. Aibéo, R.R. Pausewein, et al., Absorption edge sensitive radiography and tomography of Egyptian Papyri, J. Cult. Herit. 39 (2019) 13–20, doi:10.1016/j.culher.2019.04.007.

[15] M. Bicchieri, M. Monti, G. Piantanida, A. Sodo, All that is iron-ink is not always iron-gall!, J. Raman Spectrosc. 39 (2008) 1074–1078, doi:10.1002/jrs.1995.

[16] A. Rosalie David, H.G.M. Edwards, D.W. Farwell, D.L.A. De Faria, Raman Spectroscopic Analysis of Ancient Egyptian Pigments, Archaeometry. 43 (2001) 461–473, doi:10.1111/1475-4754.00029.

[17] R.J.H. Clark, Raman microscopy as a structural and analytical tool in the fields of art and archaeology, J. Mol. Struct 834–836 (2007) 74–80, doi:10.1016/j.molstruc.2007.01.031.

[18] S.K. Sze, N. Siddique, J.J. Sloan, R. Escribano, Raman spectroscopic characterization of carbonaceous aerosols, Atmos. Environ. 35 (2001) 561–568, doi:10.1016/S1352-2310(00)00325-3.

[19] T. Christiansen, M. Cotte, W. de Nolf, E. Mouro, J. Reyes-Herrera, S. de Meyer, et al., Insights into the composition of ancient Egyptian red and black inks on papyri achieved by synchrotron-based microanalyses, Proc. Natl. Acad. Sci. U. S. A. 117 (2020) 27825–27835, doi:10.1073/pnas.2004534117.

[20] T. Christiansen, M. Cotte, R. Loredo-Portales, P.E. Lindelof, K. Mortensen, K. Ryholt, et al., The nature of ancient Egyptian copper-containing carbon inks is revealed by synchrotron radiation based X-ray microscopy, Sci. Rep. 7 (2017) 15346, doi:10.1038/s41598-017-15652-7.

[21] F.J. Pereira, R. Lopez, M. Brasas, R. Alvarez, A.J. Aller, Synergism between SEM/EDX microanalysis and multivariate analysis for a suitable classification of Roman and Byzantine papyri, Microchem. J. 160 (2021) 105688, doi:10.1016/j.microc.2020.105688.

[22] W. Malzer, O. Hahn, B. Kanngiesser, A fingerprint model for inhomogeneous ink–paper layer systems measured with micro-x-ray fluorescence analysis, X-Ray Spectrom 33 (2004) 229–233, doi:10.1002/xrs.676.

[23] L. Heudt, D. Debois, T.A. Zimmerman, L. Köhler, F. Bano, F. Partouche, et al., Raman spectroscopy and laser desorption mass spectrometry for minimal destructive forensic analysis of black and color inkjet printed documents, Forensic Sci. Int. 219 (2012) 64–75, doi:10.1016/j.forsciint.2011.12.001.

[24] M. Strlič, L. Cséfalvayová, J. Kolar, E. Menart, J. Kosek, C. Barry, et al., Non-destructive characterisation of iron gall ink drawings: Not such a galling problem, Talanta 81 (2010) 412–417, doi:10.1016/j.talanta.2009.12.017.

[25] F. Casadio, C. Daher, L. Bellot-Gurlet, in: Raman Spectroscopy of cultural heritage Materials: Overview of Applications and New Frontiers in Instrumentation, Sampling Modalities, and Data Processing, Springer, Cham, 2017, pp. 161–211, doi:10.1007/978-3-319-52804-5_5.

[26] M. Ferrer, M.C. Sistach, Characterisation by FTIR spectroscopy of ink components in ancient manuscripts, Restaurator 26 (2005) 105–117.

[27] M. Ursescu, T. Măluţan, S. Ciovică, Iron gall inks influence on papers' thermal degradation FTIR spectroscopy applications, Eur. J. Sci. Theol. 5 (2009) 71–84.

[28] M.I. Muñoz, A.J. Aller, D. Littlejohn, The bonding of heavy metals on nitric acid-etched coal fly ashes functionalized with 2-mercaptoethanol or thioglycolic acid, Mater. Chem. Phys. 143 (2014) 1469–1480, doi:10.1016/j.matchemphys.2013.12.002.

[29] P.R. Rai, A.K. Tiwary, V. Rana, Optimization of an aqueous tablet-coating process containing carboxymethylated Cassia fistula gum, AAPS PharmSciTech 13 (2012) 431–440, doi:10.1208/s12249-012-9763-x.

[30] J. Senvaitiene, A. Beganskiene, A. Kareiva, Spectroscopic evaluation and characterization of different historical writing inks, Vib. Spectrosc. 37 (2005) 61–67, doi:10.1016/j.vibspec.2004.06.004.

[31] M.A. Castro, K. Faulds, W.E. Smith, A.J. Aller, D. Littlejohn, Identification of condensed-phase species on the thermal transformation of alkaline and alkaline earth metal sulphates on a graphite platform, Spectrochim. Acta - Part B At. Spectrosc. 59 (2004) 827–839, doi:10.1016/j.sab.2004.04.002.

[32] X. Huang, W.-D. Zhang, Preparation of Cellulose Sulphate and Evaluation of its Properties, J. Fiber Bioeng. Informatics JFBI. 3 (2010) 32–39, doi:10.3993/jfbi06201006.

[33] M.B. Wiggins, E. Heath, K.S. Booksh, J. Alcántara-García, Multi-Analytical Study of Copper-Based Historic Pigments and their Alteration Products, Appl. Spectrosc. 73 (2019) 1255–1264, doi:10.1177/0003702819856606.

[34] M. Aceto, A. Agostino, E. Boccaleri, A.C. Garlanda, The Vercelli gospels laid open: An investigation into the inks used to write the oldest Gospels in Latin, X-Ray Spectrom 37 (2008) 286–292, doi:10.1002/xrs.1047.

[35] G. Adami, A. Gorassini, E. Prenesti, M. Crosera, E. Baracchini, A. Giacomello, Micro-XRF and FT-IR/ATR analyses of an optically degraded ancient document of the Trieste (Italy) cadastral system (1893): A novel and surprising iron gall ink protective action, Microchem. J. 124 (2016) 96–103, doi:10.1016/j.microc.2015.07.020.

[36] G. Piantanida, E. Menart, M. Bicchieri, M. Strlič, Classification of iron-based inks by means of micro-Raman spectroscopy and multivariate data analysis, J. Raman Spectrosc. 44 (2013) 1299–1305, doi:10.1002/jrs.4351.

[37] A.S. Lee, V. Otieno-Alego, D.C. Creagh, Identification of iron-gall inks with near-infrared Raman microspectroscopy, J. Raman Spectrosc. 39 (2008) 1079–1084, doi:10.1002/jrs.1989.

[38] R.J. Díaz Hidalgo, R. Córdoba, P. Nabais, V. Silva, M.J. Melo, F. Pina, et al., New insights into iron-gall inks through the use of historically accurate reconstructions, Herit. Sci. 6 (2018) 1–15, doi:10.1186/s40494-018-0228-8.

[39] A.C. Ferrari, J. Robertson, Resonant Raman spectroscopy of disordered, amorphous, and diamondlike carbon, Phys. Rev. B - Condens. Matter Mater. Phys. 64 (2001) 075414, doi:10.1103/PhysRevB.64.075414.

[40] O. Hahn, B. Kanngießer, W. Malzer, X-ray fluorescence analysis of iron gall inks, pencils and coloured crayons, Stud. Conserv. 50 (2005) 23–32, doi:10.1179/sic.2005.50.1.23.

[41] H. Busemann, M.O. Alexander, L.R. Nittler, Characterization of insoluble organic matter in primitive meteorites by microRaman spectroscopy, Meteorit. Planet. Sci. 42 (2007) 1387–1416, doi:10.1111/j.1945-5100.2007.tb00581.x.

[42] O. Beyssac, J.N. Rouzaud, B. Goffé, F. Brunet, C. Chopin, Graphitization in a high-pressure, low-temperature metamorphic gradient: A Raman microspectroscopy and HRTEM study, Contrib. to Mineral. Petrol. 143 (2002) 19–31, doi:10.1007/s00410-001-0324-7.

[43] J. Kolar, A. Štolfa, M. Strlič, M. Pompe, B. Pihlar, M. Budnar, et al., Historical iron gall ink containing documents — Properties affecting their condition, Anal. Chim. Acta. 555 (2006) 167–174, doi:10.1016/J.ACA.2005.08.073.

[44] M. Pawlyta, J.N. Rouzaud, S. Duber, Raman microspectroscopy characterization of carbon blacks: Spectral analysis and structural information, Carbon N. Y. 84 (2015) 479–490, doi:10.1016/j.carbon.2014.12.030.

[45] A. Ferrari, J. Robertson, Interpretation of Raman spectra of disordered and amorphous carbon, Phys. Rev. B - Condens. Matter Mater. Phys. 61 (2000) 14095–14107, doi:10.1103/PhysRevB.61.14095.

[46] L. Bokobza, J.-L. Bruneel, M. Couzi, Raman Spectra of Carbon-Based Materials (from Graphite to Carbon Black) and of Some Silicone Composites, C 1 (2015) 77–94, doi:10.3390/c1010077.

[47] A. Sadezky, H. Muckenhuber, H. Grothe, R. Niessner, U. Pöschl, Raman microspectroscopy of soot and related carbonaceous materials: Spectral analysis and structural information, Carbon N. Y. 43 (2005) 1731–1742, doi:10.1016/j.carbon.2005.02.018.

[48] A. Coccato, J. Jehlicka, L. Moens, P. Vandenabeele, Raman spectroscopy for the investigation of carbon-based black pigments, J. Raman Spectrosc. 46 (2015) 1003–1015, doi:10.1002/jrs.4715.

[49] A.C. Ferrari, J. Robertson, Raman spectroscopy of amorphous, nanostructured, diamond-like carbon, and nanodiamond, Philos. Trans. R. Soc. A Math. Phys. Eng. Sci. 362 (2004) 2477–2512, doi:10.1098/rsta.2004.1452.

[50] M.A. Castro, A.J. Aller, K. Faulds, A.J. Aller, K. Faulds, D. Littlejohn, Study of the effect of nitric acid and metal-based chemical modifiers on graphite platform surfaces by Raman spectrometry, J. Anal. At. Spectrom. 24 (2009) 1044–1050, doi:10.1039/b905269k.

[51] Q. Pan, K. Guo, L. Wang, S. Fang, Ionic conductive copolymer encapsulated graphite as an anode material for lithium ion batteries, Solid State Ionics 149 (2002) 193–200, doi:10.1016/S0167-2738(02)00278-3.

[52] T.N. Moroz, V.A. Ponomarchuk, S.V. Goryainov, N.A. Palchik, H.G.M. Edwards, S.M. Zhmodik, Raman spectra of natural carbonaceous materials from a black shale formation, J. Raman Spectrosc. 46 (2015) 959–963, doi:10.1002/jrs.4777.

[53] C. Casiraghi, S. Pisana, K.S. Novoselov, A.K. Geim, A.C. Ferrari, Raman fingerprint of charged impurities in graphene, Appl. Phys. Lett. 91 (2007) 233108, doi:10.1063/1.2818692.

[54] D.G. Henry, I. Jarvis, G. Gillmore, M. Stephenson, Raman spectroscopy as a tool to determine the thermal maturity of organic matter: Application to sedimentary, metamorphic and structural geology, Earth-Science Rev 198 (2019), doi:10.1016/j.earscirev.2019.102936.

[55] S. Goler, J.T. Yardley, D.M. Ratzan, R. Bagnall, A. Hagadorn, J. McInerney, Dating Ancient Egyptian Papyri through Raman Spectroscopy: Concept and Application to the Fragments of the Gospel of Jesus' Wife and the Gospel of John, J. Study New Testam. 42 (2019) 98–133, doi:10.1177/0142064X19855583.

[56] S. Goler, A. Hagadorn, D.M. Ratzan, R. Bagnall, A. Cacciola, J. McInerney, et al., Using Raman spectroscopy to estimate the dates of carbon-based inks from Ancient Egypt, J. Cult. Herit. 38 (2019) 106–117, doi:10.1016/j.culher.2018.12.003.

[57] E.P. Tomasini, E.B. Halac, M. Reinoso, E.J. Di Liscia, M.S. Maier, Micro-Raman spectroscopy of carbon-based black pigments, J. Raman Spectrosc. 43 (2012) 1671–1675, doi:10.1002/jrs.4159.